2024 IEEE International Conference on Robotics and Automation (ICRA 2024)
May 13-17, 2024. Yokohama, Japan

Trajectory Optimization Strategy That Considers Body Tip-Over Stability, Limb Dynamics, and Motion Continuity in Legged Robots

Kuan-Lun Lu, I-Chia Chang, Wei-Shun Yu, and Pei-Chun Lin

Abstract— **We propose a limb trajectory planning method that considers both body and limb dynamics in robots, particularly suitable for those with non-trivial limb mass. To simplify the complexity and computation cost of using the full-body dynamics of the limbs, a reduced-order model that can simulate the dynamic characteristics of the original limb is proposed. The performance of the model is experimentally validated using an exemplary single leg-wheel of the leg-wheel transformable robot. The limb trajectory optimization is developed using a genetic algorithm that considers many aspects, including body and limb dynamics, limb workspace, limb motion continuity, body tip-over stability, and power consumption. The performance of the proposed limb trajectory planning strategy is experimentally validated using the same leg-wheel transformable robot, and the results confirm the effectiveness of the strategy.**

I. Introduction

Legged robots can move agilely across diverse terrains, but in flat terrain, their energy efficiency is far less than that of wheeled robots. Therefore, integrating the advantages of legged robots and wheeled robots can be one of the practical solutions for applications in complex terrains while maintaining energy efficiency. The concept of a leg-wheel hybrid robot is presented in various ways. [1], [2], and [3] realized the wheeled-legged concept with a similar approach in which the wheel is equipped at the foot-end joint. [4], [5], and [6] performed the concept by transforming the leg-wheel mechanism.

For both legged and leg-wheel hybrid robots, planning and controlling leg motion are essential and crucial tasks. Most studies implement force or compliance force control on the stance legs, and position control on the swing legs. For the foot-end trajectory of the swing leg, numerous researchers have formulated the foot-end trajectory with different types of curves, such as polynomial, Bezier, and sinusoidal-like. [7] proposed a bionic impact-free foot-end trajectory, adopting quintic polynomial curves for the back and forward swings and cycloid curves for the stride trajectory. [8] planned a foot-end trajectory for quadruped robots with a high-speed trot gait. The foot-end trajectory was planned as a spline curve, ensuring continuity of position, speed, and acceleration during a high-speed trot gait. [9] designed a smooth foot-end trajectory with Bezier curves, achieving the continuity of velocity and acceleration with the design of the control points of Bezier curves. [10] found an optimal, efficient gait over a range of retraction rates and reduced slippage and impact at the moment of touchdown. [11] proposed an ellipse-based trajectory method to generate foot-end trajectories for a gallop gait, and the results were effective in achieving a stable gallop gait.

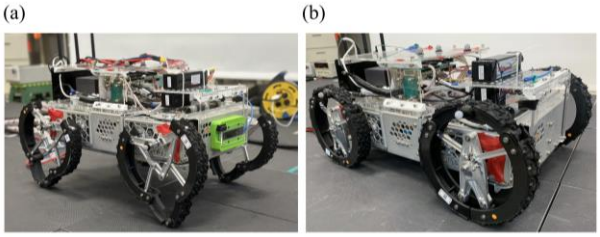

Fig. 1. The photo of the leg-wheel transformable robot with linkage-based leg-wheel mechanisms in leg mode (a) and wheel mode (b).

The leg-wheel transformable robot utilized in this study was developed in the lab, as shown in Figure 1 [12]. The legged and wheeled forms of the robot are achieved by transforming the 11-linkage mechanism [13]. The robot in legged mode has a leg length that is 3.4 times the wheel radius, significantly increasing its rough terrain negotiability. By contrast, the robot in wheeled mode performs fast, smooth, and power-efficient motions on flat terrain. Owing to the complex leg-wheel design, the leg wheel itself has non-trivial mass and inertia; thus, its motion affects body motion, especially when all leg wheels are in motion. Therefore, the motion planning of the leg-wheel is a crucial task that should be carefully addressed.

In this study, we propose a trajectory planning strategy that simultaneously considers the dynamics of the body and leg wheels. On the leg-wheel side, mechanical properties such as the mass and inertia of the leg-wheel are included in the construction of reduced-order leg-wheel modeling. The leg-wheel trajectory itself also follows the requirements of velocity and acceleration continuity. On the body side, whole-body stability is considered. By combining all of these criteria and constraints and optimizing the process for energy efficiency, the desired leg-wheel motion trajectory of the robot is obtained. Compared to motion planning using the whole-body dynamics expected in the humanoid community, this methodology is rare in the multi-legged robot community. Further, owing to the complexity of the leg wheel, in contrast to the humanoid community that uses the original morphology of the robot for optimization, here, the reduced-order model of the leg wheel is developed to extract its essential motion dynamics for trajectory optimization. To the best of our knowledge, this is the first work to plan leg/wheel trajectories of the robot in the legged/hybrid robot community.

This work is supported by the National Science and Technology Council, Taiwan, under contract: MOST 110-2221-E-002-111-MY3.

The authors are with the Department of Mechanical Engineering, National Taiwan University (NTU), No.1 Roosevelt Rd. Sec.4, Taipei 106, Taiwan. (Corresponding email: peichunlin@ntu.edu.tw).

The remainder of this paper is organized as follows. Section II describes the dynamics of the linkage-based leg-wheel mechanism used in this study. Section III presents the optimization method for leg-wheel trajectories in swings. Section IV describes the experimental results and discussion, and Section V concludes the work.

II. The Robot

A. The Robot Specifications

Figure 1 shows the leg-wheel transformable robot utilized in this research [12] [14] [15] [16]. The robot was equipped with four leg-wheel modules. Each module was actuated with two brushless DC motors. The front modules were connected to an Ackermann steering mechanism, enabling the robot to achieve steering in wheel mode. The body's weight, including the battery, was 21.205 kg, and the weight of the leg-wheel module was 0.654 kg. The robot's body measured 0.33 m in width, 0.62 m in length, 0.134 m in height, and 0.444 m in wheelbase. The wheel diameter was 0.2 m, and the maximum length of the leg wheel was 0.34 m.

B. The Leg-Wheel Kinematics

Figure 2 shows the configuration of the leg wheel and the associated notations. The leg-wheel module had two degrees of freedom: one of the motors controls the right linkage (OA), and the other controls the left linkage (OA'). We defined the state of the motor angle as $\boldsymbol{\Phi} = [\phi_R \quad \phi_L]^T$. For a simpler analysis and representation, we established another coordinate $\boldsymbol{\Theta} = [\theta \quad \beta]^T$, where the length of the leg wheel only depended on θ and the orientation of the leg wheel only depended on β:

$$\boldsymbol{\Theta} = \begin{bmatrix}\theta \\ \beta\end{bmatrix} = \frac{1}{2}\begin{bmatrix}1 & -1 \\ 1 & 1\end{bmatrix}\begin{bmatrix}\phi_R \\ \phi_L\end{bmatrix} + \begin{bmatrix}1 \\ 0\end{bmatrix}\theta_0 \tag{1}$$

In other words, the notation resembled the toe of the leg wheel in polar coordinates. When the leg wheel was in wheel mode (i.e., $\theta = \theta_0 = 17°$), it had the shortest length of 0.1 m, equal to the wheel radius. From the $\boldsymbol{\Theta}$ coordinate definition, the kinematic model of the leg wheel was derived by geometric method, and the Jacobian matrix $\boldsymbol{J_G}$ of point G was obtained by central finite difference approximation.

C. The Reduced-Order Dynamic Model of the Leg-Wheel

The leg wheel was an 11-linkage closed-chain mechanism, and the complex formulation of its dynamic equations resulted in high computational costs in the optimization process. Therefore, we proposed a reduced-order model of the leg wheel that simplifies the variation of the center of mass (COM) position with respect to the hip point O and inertia with respect to COM of the leg wheel using polynomial approximations with θ as the solo variable, $R_m(\theta)$ and $I_c(\theta)$, as shown in Figure 3:

$$\begin{aligned} R_m(\theta) &= A_4\theta^4 + A_3\theta^3 + A_2\theta^2 + A_1\theta + A_0 \\ I_c(\theta) &= B_4\theta^4 + B_3\theta^3 + B_2\theta^2 + B_1\theta + B_0 \end{aligned} \tag{2}$$

Since θ and β controlled the leg wheel's length and angle, respectively, the leg wheel was analogized to a revolute-prismatic manipulator, where the state vector of the leg wheel was defined as $\boldsymbol{q} = [R_m \quad \beta]^T$. The transformation between state $\boldsymbol{q}$ and state $\boldsymbol{\Theta}$ was obtained by Jacobian matrices:

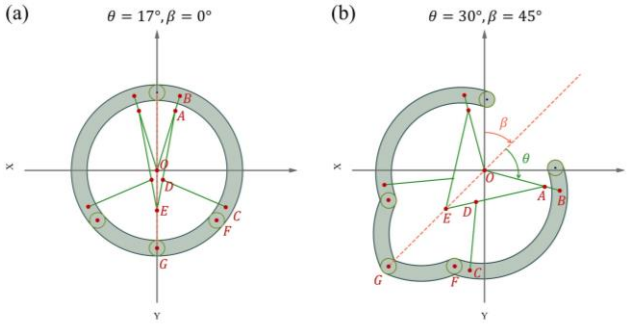

Fig. 2. The leg-wheel in wheeled mode (a) and in legged mode (b). The leg-wheel rim is composed of four circular arcs.

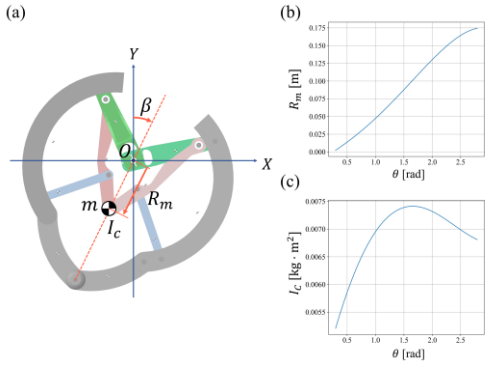

Fig. 3. The leg-wheel module: (a) Notations utilized in deriving the reduced-order model of the leg wheel, (b) the COM with respect to the hip point O, $R_m(\theta)$, and (c) the inertia with respect to the COM, $I_c(\theta)$,

$$\dot{\boldsymbol{q}} = \boldsymbol{J_\Theta}\dot{\boldsymbol{\Theta}} = \begin{bmatrix}4A_4\theta^3 + 3A_3\theta^2 + 2A_2\theta + A_1 & 0 \\ 0 & 1\end{bmatrix}\begin{bmatrix}\dot{\theta} \\ \dot{\beta}\end{bmatrix} \tag{3}$$

$$\begin{aligned}\ddot{\boldsymbol{q}} = \boldsymbol{J_{\Theta\Theta}}\dot{\boldsymbol{\Theta}}^2 + \boldsymbol{J_\Theta}\ddot{\boldsymbol{\Theta}} &= \begin{bmatrix}12A_4\theta^2 + 6A_3\theta + 2A_2 & 0 \\ 0 & 1\end{bmatrix}\begin{bmatrix}\dot{\theta}^2 \\ \dot{\beta}^2\end{bmatrix} \\ &+ \begin{bmatrix}4A_4\theta^3 + 3A_3\theta^2 + 2A_2\theta + A_1 & 0 \\ 0 & 1\end{bmatrix}\begin{bmatrix}\ddot{\theta} \\ \ddot{\beta}\end{bmatrix}\end{aligned} \tag{4}$$

The dynamic equations of the reduced-order model of the leg-wheel are derived using the Lagrangian Method. The Euler-Lagrange equations are shown in (5), where T, V, and L represent kinetic energy, potential energy, and Lagrangian, respectively.

$$\begin{aligned} L &= T - V \\ \tau &= \frac{d}{dt}\left(\frac{\partial L}{\partial \dot{q}}\right) - \left(\frac{\partial L}{\partial q}\right) \end{aligned} \tag{5}$$

The total kinetic energies and potential energies of the system were as follows:

$$\begin{aligned} T &= \frac{1}{2}m\left(\left(R_m\dot{\beta}\right)^2 + \left(\dot{R_m}\right)^2\right) + \frac{1}{2}I_c\dot{\beta}^2 \\ V &= -mgR_m\cos\beta \end{aligned} \tag{6}$$

The equation of motion was derived as follows:

$$\begin{bmatrix} F_{R_m} \\ \tau_\beta \end{bmatrix} = \begin{bmatrix} m & 0 \\ 0 & I_c + mR_m^2 \end{bmatrix} \begin{bmatrix} \ddot{R_m} \\ \ddot{\beta} \end{bmatrix} + \begin{bmatrix} -mR_m\dot{\beta}^2 \\ 2mR_m\dot{R_m}\dot{\beta} + \dot{I_C}\dot{\beta} \end{bmatrix} + \begin{bmatrix} -mg\cos\beta \\ mgR_m\sin\beta \end{bmatrix} \quad (7)$$

By applying the law of conservation of energy, the transformation between $[F_{R_m} \quad \tau_\beta]^T$ and the motor actuate torque $[\tau_{\phi_R} \quad \tau_{\phi_L}]^T$ was derived as:

$$\dot{\boldsymbol{\Theta}} = J_\Phi \dot{\boldsymbol{\Phi}} \quad (8)$$

$$\begin{bmatrix} F_{R_m} \\ \tau_\beta \end{bmatrix} = \left(\boldsymbol{J_\Theta}^T\right)^{-1} \left(\boldsymbol{J_\Phi}^T\right)^{-1} \begin{bmatrix} \tau_{\phi_R} \\ \tau_{\phi_L} \end{bmatrix} \quad (9)$$

The forward and inverse dynamic model of the leg wheel was then obtained in a computation-efficient manner using (7)(8)(9)

D. Validation of the Reduced-Order Dynamic Model of the Leg-Wheel

Figure 4 shows a single-leg platform designed to validate the leg wheel's dynamic behavior. The single-leg module was attached to two parallelly-installed rails with linear bearings, which constrained the movement of the leg-wheel module on the vertical axis. A single-axis load cell was connected to the leg-wheel module, which measured the vertical axial force of the leg-wheel module while the leg wheel was swinging.

The validation experiment was performed by giving the control inputs of the leg wheel's sinusoidal position trajectories (θ, β), where the leg wheel tracked the trajectory using field-oriented position control. The state (θ, β) were transformed into state (R_m, β) using (2)(3)(4). Next, by the dynamic equation (7), the (F_{R_m}, τ_β) trajectory was obtained, which represents the constraint force and constraint torque to hold the dynamic constraint. Furthermore, the required joint torque was computed by substituting the (F_{R_m}, τ_β) to $(\tau_{\phi_R}, \tau_{\phi_L})$.

Figure 5 shows the validation results. The reduced-order dynamic model of the leg wheel effectively estimated the constraint force while the leg wheel was swinging. The required motor current for the given trajectory was also calculated. There was a slight error between the measured current in the experiment and the estimated current using the dynamic model, possibly caused by current sensor noise, friction force in the gearbox, and numerous joint bearings in the leg wheel. The dynamic model was sufficiently accurate to estimate the energy requirements of the trajectory. Furthermore, the load cell measurement revealed that the inertia force caused by the leg motion was sufficient to affect the robot's motion. Therefore, we propose an optimization method that considers swing leg dynamics to obtain the optimal foot-end trajectory for the swing legs.

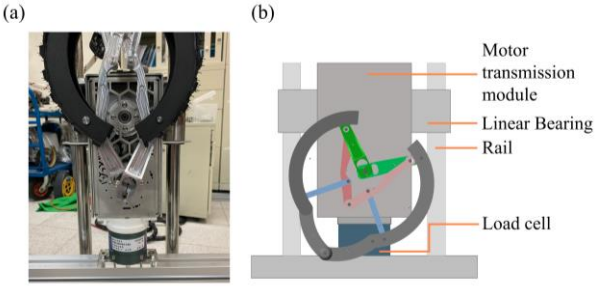

Fig. 4. The single-leg platform validating the performance of the reduced-order dynamic model: (a) A photo and (b) the associated notations.

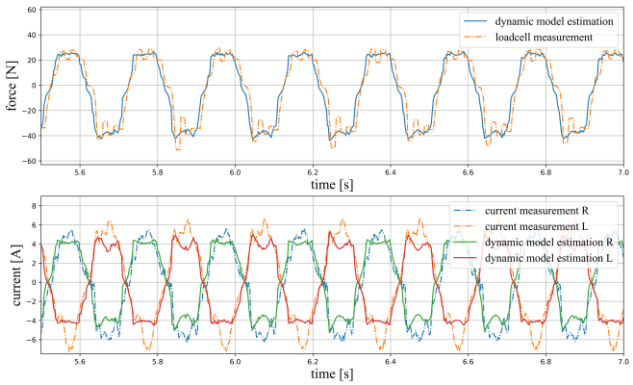

Fig. 5. The comparison of the force/current measured during the leg-wheel experiment and those estimated by the reduced-order model. In this set of experiment, $\theta(t) = \frac{\pi}{4}\sin\left(\frac{2\pi}{5}t\right) + \frac{\pi}{2}$ and $\beta(t) = 0$.

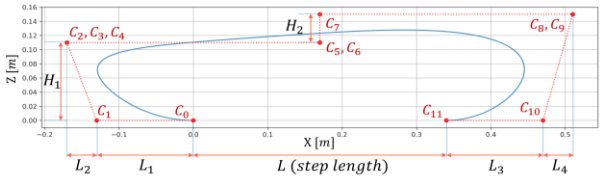

Fig. 6. The leg-wheel trajectory parametrized using a Bezier curve with twelve control points.

III. The Leg-Wheel Trajectory Optimization

Planning limb trajectories is a critical task in legged robots. A trajectory generator developed for high-speed locomotion for MIT Cheetah is a classic example [9], in which the stance phase trajectory and the swing phase trajectory are designed separately. The former is designed based on compliant force control, and the latter is based on position control. The trajectory was parametrized by a Bezier curve with 12 control points, with the number of points being sufficient to grant ground clearance, lift-off, touchdown velocity, acceleration, etc. Following this approach, we parametrized the Bezier curve using 12 control points. Together with the designated step length L and swing period T_{sw}, the leg-wheel trajectory was effectively optimized.

A. The Bezier Curve Parametrization

The Bezier curve utilized in this work is defined by 12 control points [9]. Considering that the lift-off and touch-down vertical velocity should be zero and the smooth force transition between "follow-through," "protraction," and "retraction," the

12 control points were parametrized with 6 variables $\boldsymbol{b} = [H_1\ H_2\ L_1\ L_2\ L_3\ L_4]$, as shown in Figure 6. Double-overlapped control points generate zero velocity, and triple-overlapped control points cause zero acceleration. The overlapped control points were set such that the trajectory fit the consideration of velocity and smooth force transition.

B. The Optimization Problem Formulation

This work aimed to achieve an optimal Bezier-based foot-end trajectory for all four leg wheels so that the robot could obtain the maximum tip-over stability margin and the least energy consumption. Furthermore, the trajectory of the swing leg wheel was designed to satisfy workspace constraints and the continuity of velocity and acceleration.

The state of the robot is defined as follows:

$$\begin{aligned} \boldsymbol{X_k} &= [\dot{\boldsymbol{x}}_k\ \boldsymbol{x}_k\ \boldsymbol{\omega}_k\ \boldsymbol{h}_k\ \boldsymbol{q}_{LF}\ \boldsymbol{q}_{RF}\ \boldsymbol{q}_{RH}\ \boldsymbol{q}_{LH}]^T \\ \boldsymbol{U_k} &= [\boldsymbol{\tau}_{LF_k}\ \boldsymbol{\tau}_{RF_k}\ \boldsymbol{\tau}_{RH_k}\ \boldsymbol{\tau}_{LH_k}]^T \end{aligned} \tag{10}$$

The $\boldsymbol{X}_k$ represent the state of the robot, where $\boldsymbol{x}_k$, $\boldsymbol{\omega}_k$, $\boldsymbol{h}_k$, and $\boldsymbol{q}$ represent the position of the robot COM, the orientation of the robot in quaternion, the angular velocity, and the joint state of each leg, respectively. The $\boldsymbol{U}_k$ represents the torque inputs of the leg wheels. The optimal problem was formulated as follows:

$$\begin{aligned} \text{minimize} \quad & \sum_{k}^{N-1} V(\boldsymbol{X}_k, \boldsymbol{U}_k) + V_T(\boldsymbol{X}_N) \\ \text{subject to} \quad & \boldsymbol{X}_{k+1} = g(\boldsymbol{X}_k, \boldsymbol{U}_k) \\ & \boldsymbol{X}_k \in \mathbb{X}, k = 1,2,\dots,N \\ & \boldsymbol{U}_k \in \mathbb{U}, k = 1,2,\dots,N-1 \end{aligned} \tag{11}$$

where $V(\boldsymbol{X}_k, \boldsymbol{U}_k)$ represents the integral objective function and $V_T(\boldsymbol{X}_N)$ represents the terminal objective function, including the evaluation of tip-over stability and energy consumption. $g(\boldsymbol{X}_k, \boldsymbol{U}_k)$ represents the state equation of the robot, including the single rigid body dynamic model and the leg-wheel dynamic model. $\mathbb{X}$ represents the feasible set of the state of the robot, and $\mathbb{U}$ represents the feasible set of torque inputs for each leg. Given step length L, swing period T_{sw}, and Bezier curve profiles of the leg wheels $\boldsymbol{B} = [\boldsymbol{b}_{LF}\ \boldsymbol{b}_{RF}\ \boldsymbol{b}_{RH}\ \boldsymbol{b}_{LH}]$, the optimal foot-end trajectories profile for the leg wheels $\boldsymbol{B}^*$ was computed.

C. The Tip-Over Stability Measure

In various studies of legged robots, robot walking stability is often characterized by the concept of a support polygon. The robot tips over when the rigid COM falls out of the support polygon. [17] proposed a force-angle tip over stability margin measure for mobile manipulators. The measure of stability proposed could authentically reflect whether the robot is in a state of tipping.

For the leg-wheel transformable robot utilized in this study, the forces ($\boldsymbol{f}$) and moments ($\boldsymbol{n}$) acting on the robot COM that would participate in tip-over instability were expressed as:

$$\begin{aligned} \boldsymbol{f_r} &= \sum \boldsymbol{f_{grav}} + \sum \boldsymbol{f_{sw}} + \sum \boldsymbol{f_{dist}} - \sum \boldsymbol{f_{inetial}} \\ &= -\sum \boldsymbol{f_{support}} \end{aligned} \tag{12}$$

$$\boldsymbol{n_r} = \sum \boldsymbol{n_{sw}} + \sum \boldsymbol{n_{dist}} - \sum \boldsymbol{n_{inertial}} = -\sum \boldsymbol{n_{support}} \tag{13}$$

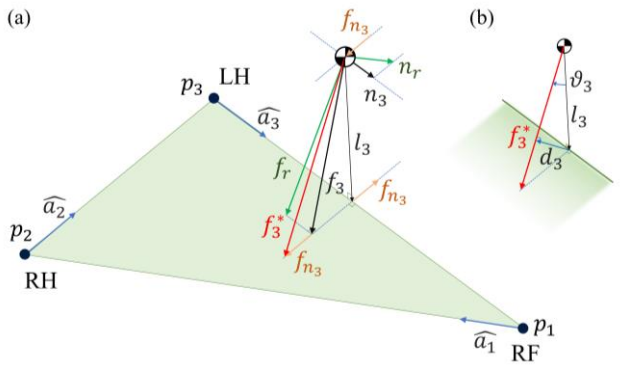

Fig. 7. Force-angle stability analysis of the robot in walking. At this moment, the right front (RF), right hind (RH), and left hind (LH) legs are in stance, forming a support polygon. (a) $\boldsymbol{f_3}$ and $\boldsymbol{n_3}$ are the effective components of the resultant force $\boldsymbol{f_r}$ and the resultant moment $\boldsymbol{n_r}$ to the tip over motion with respect to the axis $\widehat{\boldsymbol{a_3}}$, one of the axes forming the support polygon. The $\boldsymbol{f_3^*}$ is the net effective force which sums the effect of $\boldsymbol{f_3}$ and $\boldsymbol{n_3}$, where ϑ represents the effective force angle as shown in (b).

where f_{grav} represents the gravitational loads, $\boldsymbol{f_{sw}}$ and $\boldsymbol{n_{sw}}$ represent the force and moment transmitted from the swinging leg, respectively. The symbols $\boldsymbol{f_{support}}$ and $\boldsymbol{n_{support}}$ represent the ground reaction force and the moment caused by the ground reaction force. The symbols $\boldsymbol{f_{dist}}$ and $\boldsymbol{n_{dist}}$ represent force and torque from the external disturbances acting on the system. The symbols $\boldsymbol{f_{inetial}}$ and $\boldsymbol{n_{inertial}}$ are the inertial force and moment, respectively. As shown in Figure 7(a), the components of resultant force $\boldsymbol{f_r}$ and moment $\boldsymbol{n_r}$ that would contribute to tip over with respect to the axis $\widehat{\boldsymbol{a_i}}$ was derived as:

$$\boldsymbol{f_i} = \left(\mathbf{I} - \widehat{\boldsymbol{a_i}}\widehat{\boldsymbol{a_i}}^T\right)\boldsymbol{f_r} \tag{14}$$

$$\boldsymbol{n_i} = \left(\widehat{\boldsymbol{a_i}}\widehat{\boldsymbol{a_i}}^T\right)\boldsymbol{n_r} \tag{15}$$

The angular loads $\boldsymbol{n_i}$ were replaced with equivalent force couple as follows:

$$\boldsymbol{f_{n_i}} = \frac{\widehat{\boldsymbol{l_i}} \times \boldsymbol{n_i}}{\|\boldsymbol{l_i}\|} \tag{16}$$

Combining the effective force component and the equivalent force couple of the effective moment components, the effective net force vector for the tip-over axis, $\boldsymbol{f_i^*}$ was formulated as follows:

$$\boldsymbol{f_i}^* = \boldsymbol{f_i} + \boldsymbol{f_{n_i}} \tag{17}$$

Next, the force-angle stability measure S is then defined as:

$$S = \vartheta_i \cdot \|\boldsymbol{d_i}\| \cdot \|\boldsymbol{f_i^*}\| \tag{18}$$

where $\|\boldsymbol{d_i}\|$ represents the distance between $\boldsymbol{f_i^*}$ and tip-over axis, and ϑ_i represents the force-angle of $\boldsymbol{f_i^*}$, as shown in Figure 7 (b). A positive S indicates that $\boldsymbol{f_i^*}$ is directed inside the support polygon and, thus, a high tip-over stability. The magnitude of S also indicates a stable system's tip-over stability margin. Critical tip-over stability occurs when $S = 0$. Tip-over instability occurs when $\boldsymbol{f_i^*}$ is directed outside the support polygon, in which case S is negative.

D. The Objective Function Definition

From the definition of the tip-over stability measure in (18)(19), the desired tip-over stability measure should be positive, and the magnitude should be as large as possible. As for the energy efficiency, by using the reduced-order dynamic model shown in (7)(8)(9), the required torque for tracking a given Bezier curve was obtained. The overall objective function was defined as follows:

$$V(\boldsymbol{X}_k, \boldsymbol{U}_k) = \sum_{k}^{N-1} (-W_s \cdot \theta_i \cdot \|\boldsymbol{d_i}\| \cdot \|\boldsymbol{f_i^*}\| + \boldsymbol{u}^T \boldsymbol{W_u} \boldsymbol{u}) \cdot \Delta t \quad (19)$$

where $\boldsymbol{u}$ represent the required torque vector, W_s and $\boldsymbol{W_u}$ represent the weight of tip over stability and energy consumption, respectively.

E. The Constraints of the Leg-Wheel Trajectory

The leg-wheel trajectory was optimized to satisfy several constraints, including the leg wheel's workspace and the velocity and acceleration continuity at the moments of liftoff and touchdown when the stance trajectory and swing trajectory were switched. The minimum and maximum lengths of the leg wheel were 0.1 m and 0.3428 m, respectively. Moreover, to prevent the leg wheels from colliding, they must not exceed the coronal plane of the robot body. Thus, the workspace constraint was represented as follows:

$$0.1 \leq \left\| \boldsymbol{P_G}(t) - \boldsymbol{P_{hip}}(t) \right\| \leq 0.3428 \quad (20)$$

At the moments of lift-off and touch-down, the position, velocity, and acceleration of the toe point G of the leg wheel, as shown in Figure 2(b), should be continuous, as follows:

$$\boldsymbol{P_G}|_{t_{sw}=0} = \boldsymbol{P_G}|_{t_{st}=T_{st}}, \boldsymbol{P_G}|_{t_{sw}=\mathrm{T_{sw}}} = \boldsymbol{P_G}|_{t_{st}=0} \quad (21)$$

$$\dot{\boldsymbol{P}}_{\boldsymbol{G}}|_{t_{sw}=0} = \dot{\boldsymbol{P}}_{\boldsymbol{G}}|_{t_{st}=T_{st}}, \dot{\boldsymbol{P}}_{\boldsymbol{G}}|_{t_{sw}=\mathrm{T_{sw}}} = \dot{\boldsymbol{P}}_{\boldsymbol{G}}|_{t_{st}=0} \quad (22)$$

$$\ddot{\boldsymbol{P}}_{\boldsymbol{G}}|_{t_{sw}=0} = \ddot{\boldsymbol{P}}_{\boldsymbol{G}}|_{t_{st}=T_{st}}, \ddot{\boldsymbol{P}}_{\boldsymbol{G}}|_{t_{sw}=\mathrm{T_{sw}}} = \ddot{\boldsymbol{P}}_{\boldsymbol{G}}|_{t_{st}=0} \quad (23)$$

where T_{sw} and T_{st} represent the period of swing phase and stance phase, respectively, and t_{st} and t_{sw} represent the elapsed time after lift-off and touch-down, respectively.

F. Optimization Implementation

To obtain the optimal leg-wheel swing trajectory, the optimal problem was solved using genetic algorithms (GA). GA offers several advantages for global optimization, such as (1) applicability to a wide range of optimization problems, including those with non-linear, complex objective functions, and (2) less likelihood of getting stuck in local optima compared to traditional optimization methods.

The chromosome used in the GA presented 24 genes ($\boldsymbol{B} = [\boldsymbol{b}_{LF_{1\times6}}\ \boldsymbol{b}_{RF_{1\times6}}\ \boldsymbol{b}_{RH_{1\times6}}\ \boldsymbol{b}_{LH_{1\times6}}]$). The specific parameters set up for the GA are shown in Table 1. The optimal trajectory parameters $\boldsymbol{B}^*$ was derived by implementing a GA with the dynamic model simulations that provided fitness for evaluation. The constraint violation of chromosomes was set as a penalty to fitness to achieve the optimal solution that satisfied the constraints.

TABLE I. PARAMETERS OF GENETIC ALGORITHM

Parameters of genetic algorithm	
Chromosome length	24
Population size	60
Number of offspring	30
Sampling method	Random Sampling
Crossover	Simulated Binary Crossover (Probability = 0.9)
Mutation	Polynomial Mutation
Evolution generations	200

IV. THE RESULTS AND DISCUSSION

The Robot experiments were conducted to validate the proposed leg-wheel trajectory optimization strategy. The robot was set to walk with step length $L = 0.2$ m, swing period $T_{sw} = 0.6$ s, and at least a foot lift of 0.03 m. The robot was set to walk straight at a constant speed and without variations in height. In addition to test the optimal trajectory, the trajectory before optimization was evaluated as the baseline. A motion capture system (Vicon) was utilized to record the robot's motion with a sampling of 500 Hz as the ground truth.

The robot's high-level controller was realized by position control, and each joint controller was realized by FOC-based torque control. The high-level controller operated in the embedded controller (SbRIO-9629, National Instruments (NI), 1000 Hz hardware interrupt), and the low-level joint controller operated in the microcontroller unit (STM32-F446RE, 40 kHz hardware interrupt). Communication between the embedded controller and the joint controller unit was realized by the CAN bus. The power inputs to each BLDC motor were monitored with a current sensor at 1000 Hz.

A. The Leg-Wheel Trajectory Optimization

For the first generation of chromosomes, the trajectories for each leg were configured as shown in Figure 8(a). The optimized trajectories obtained after 200 generations of evolution are shown in Figure 8(b). Figure 9 shows the improvement in the tip-over stability measure in the simulation after optimization. Tip-over instability occurred when implementing the first-generation trajectories. However, the tip-over stability measure of the optimized trajectory was primarily positive, indicating that the robot was mostly stable. Moreover, critical tip-over stability (tip-over stability equals zero) occurred at the moment of switching the foot, such that the robot achieved a smoother transition between each step.

B. The Experimental Results

The robot was set to track a straight forward trajectory with 0.083 m/s velocity. Figure 10 shows the robot's performance with leg-wheel trajectories before and after optimization. The orientation of the robot is expressed in Tait-Bryan angles (z-y-x). While the tracking errors of $\boldsymbol{P}_{COM_X}$ were not significantly improved, those of $\dot{\boldsymbol{P}}_{COM_X}$ had a remarkable improvement in both the smoothness and the tracking error. The average velocity tracking error was reduced from 0.103 m/s to 0.0317 m/s. The robot with optimized leg-wheel trajectories exhibited substantially reduced tracking errors in pitch and roll during a certain period of the gait pattern. The average tracking error of

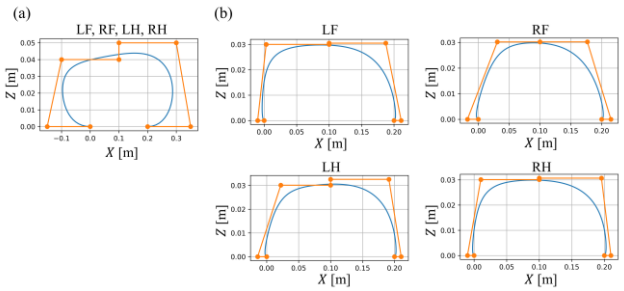

Fig. 8. The leg-wheel trajectories in its motion plane: (a) The initial trajectory of leg-wheels (i.e., unoptimized) and (b) the trajectories of the leg-wheels after optimization using GA.

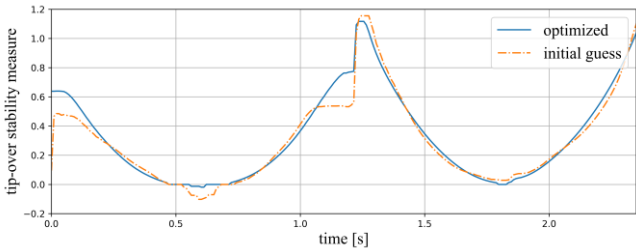

Fig. 9. The tip-over stability measure of the robot operating with leg-wheel trajectories before (i.e., dash-dotted orange curve) and after optimization (i.e., solid blue curve). The tip-over stability measure of the robot with unoptimized trajectories is negative around 0.6s, which indicates instability occurs.

the roll angle decreased from 0.038 rad to 0.0266 rad, and the average tracking error of the pitch angle slightly reduced from 0.032 rad to 0.03 rad.

Figure 10 shows the power consumption of the robot. The robot consumed less power with the optimized leg-wheel trajectories than with the trajectories before optimization. The average power consumption was reduced from 220 W to 134 W, and the power profile of the robot with the leg-wheel optimization was much smoother than without the optimization.

V. Conclusion and Future Work

In this study, we proposed a limb trajectory planning method for the robot that considers both body and limb dynamics. Including leg-wheel dynamics in trajectory planning is crucial for robots with non-trivial limb masses. To remedy the complexity and computation costs of using the full-body dynamics of the limbs, a reduced-order model that can simulate the dynamic characteristics of the original limb was proposed. The performance of the reduced-order model was experimentally validated using a single leg-wheel module, and the results confirmed the model's effectiveness. The results showed that the inertial force of the leg wheel caused by its swing motion significantly affected the motion of the robot's body.

We performed leg-wheel trajectory optimization that considered many issues, including body and leg-wheel dynamics, leg-wheel workspace, leg-wheel motion continuity, body tip-over stability, and power consumption. The GA was adopted for optimization. The performance of the proposed strategy was experimentally validated, and the leg-wheel trajectory before optimization was utilized as the baseline. The

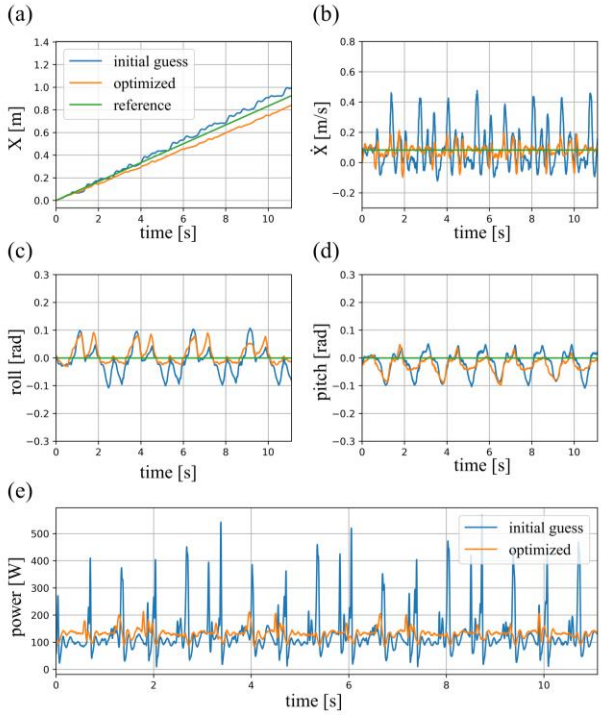

Fig. 10. The performance of the robot with leg-wheel trajectories before (i.e., blue solid curves) and after (i.e., orange solid curves) optimization. (a)–(e) separately shows forward displacement ($\boldsymbol{P}_{COM_X}$), forward velocity ($\dot{\boldsymbol{P}}_{COM_X}$), roll, pitch, and power versus time

experimental results confirmed that the optimized leg-wheel trajectory increased the performance of the robot in both motion smoothness and power consumption. The velocity tracking error decreased by 70.3%, and the power consumption was reduced by 39.1%.

We plan to realize the optimization process with a more efficient computational method to generate optimal leg-wheel trajectories online. Incorporating the terrain into the optimization considerations by integrating the point cloud information allows the technique proposed in this study to be more closely aligned with practical scenarios.

References

[1] M. Bjelonic et al., "Keep rollin'—whole-body motion control and planning for wheeled quadrupedal robots," IEEE Robotics and Automation Letters, vol. 4, no. 2, pp. 2116-2123, 2019.

[2] A. Laurenzi, E. M. Hoffman, and N. G. Tsagarakis, "Quadrupedal walking motion and footstep placement through linear model predictive control," in 2018 IEEE/RSJ International Conference on Intelligent Robots and Systems (IROS), 2018: IEEE, pp. 2267-2273.

[3] T. Klamt and S. Behnke, "Anytime hybrid driving-stepping locomotion planning," in 2017 IEEE/RSJ International Conference on Intelligent Robots and Systems (IROS), 2017: IEEE, pp. 4444-4451.

[4] R. Cao, J. Gu, C. Yu, and A. Rosendo, "Omniwheg: An omnidirectional wheel-leg transformable robot," in 2022 IEEE/RSJ International Conference on Intelligent Robots and Systems (IROS), 2022: IEEE, pp. 5626-5631.

[5] S.-C. Chen, K.-J. Huang, W.-H. Chen, S.-Y. Shen, C.-H. Li, and P.-C. Lin, "Quattroped: a leg--wheel transformable robot," IEEE/ASME Transactions On Mechatronics, vol. 19, no. 2, pp. 730-742, 2013.

[6] W.-H. Chen, H.-S. Lin, Y.-M. Lin, and P.-C. Lin, "TurboQuad: A novel leg–wheel transformable robot with smooth and fast behavioral transitions," IEEE Transactions on Robotics, vol. 33, no. 5, pp. 1025-1040, 2017.

[7] S. Wang, K. Ma, X. Deng, and X. Liao, "Quadruped Robot Foot-end Trajectory Generation Algorithm," in 2022 2nd International Conference on Computation, Communication and Engineering (ICCCE), 2022: IEEE, pp. 114-119.
[8] X. Zeng, S. Zhang, H. Zhang, X. Li, H. Zhou, and Y. Fu, "Leg trajectory planning for quadruped robots with high-speed trot gait," Applied Sciences, vol. 9, no. 7, p. 1508, 2019.
[9] D. J. Hyun, S. Seok, J. Lee, and S. Kim, "High speed trot-running: Implementation of a hierarchical controller using proprioceptive impedance control on the MIT Cheetah," The International Journal of Robotics Research, vol. 33, no. 11, pp. 1417-1445, 2014.
[10] M. Haberland, J. D. Karssen, S. Kim, and M. Wisse, "The effect of swing leg retraction on running energy efficiency," in 2011 IEEE/RSJ International Conference on Intelligent Robots and Systems, 2011: IEEE, pp. 3957-3962.
[11] K. Y. Kim and J. H. Park, "Ellipse-based leg-trajectory generation for galloping quadruped robots," Journal of mechanical science and technology, vol. 22, pp. 2099-2106, 2008.
[12] H.-Y. Wang, L.-J. Chen, W.-S. Yu, and P.-C. Lin, "A Wheel to Leg Transformation Strategy in a Leg-Wheel Transformable Robot," in 2023 IEEE/ASME International Conference on Advanced Intelligent Mechatronics (AIM), 2023: IEEE, pp. 293-298.
[13] H.-Y. Chen, T.-H. Wang, K.-C. Ho, C.-Y. Ko, P.-C. Lin, and P.-C. Lin, "Development of a novel leg-wheel module with fast transformation and leaping capability," Mechanism and Machine Theory, vol. 163, p. 104348, 2021.
[14] L.-J. Chen and P.-C. Lin, "Gait Pattern Stabilization using Central Pattern Generator with Foothold Force Optimization for Quadruped Robots," in 2022 IEEE/ASME International Conference on Advanced Intelligent Mechatronics (AIM), 2022: IEEE, pp. 1658-1663.
[15] Y.-J. Liu and P.-C. Lin, "Development of a dynamic model of the 11-linkage and closed-chain leg-wheel module," presented at the 2022 IEEE/ASME International Conference on Advanced Intelligent Mechatronics (AIM), Sapporo, Japan, 2022. [Online]. Available: https://doi.org/10.1109/AIM52237.2022.9863328.
[16] Y.-C. Zhuang, Y.-J. Liu, W.-S. Yu, and P.-C. Lin, "A Hybrid Impedance and Admittance Control Strategy for a Shape-Transformable Leg-Wheel," in 2023 IEEE/ASME International Conference on Advanced Intelligent Mechatronics (AIM), 2023: IEEE, pp. 299-304.
[17] E. Papadopoulos and D. A. Rey, "The force-angle measure of tipover stability margin for mobile manipulators," Vehicle System Dynamics, vol. 33, no. 1, pp. 29-48, 2000.